# Sensing nitrous oxide with QCL-coupled silicon-on-sapphire ring resonators

**Clinton J. Smith,[1,*] Raji Shankar,[2] Matthew Laderer,[1] Michael B. Frish,[1] Marko Lončar,[2] and Mark G. Allen[1]**

[1]*Physical Sciences, Inc., 20 New England Business Center, Andover, MA 01810, USA*
[2]*School of Engineering and Applied Sciences, Harvard University, Cambridge, MA 02138, USA*
[*]*csmith@psicorp.com*

**Abstract:** We report the initial evaluation of a mid-infrared QCL-coupled silicon-on-sapphire ring resonator gas sensor. The device probes the $N_2O$ 2241.79 $cm^{-1}$ optical transition (R23 line) in the $\nu_3$ vibrational band. $N_2O$ concentration is deduced using a non-linear least squares fit, based on coupled-mode theory, of the change in ring resonator $Q$ due to gas absorption losses in the evanescent portion of the waveguide optical mode. These early experiments demonstrated response to 5000 ppmv $N_2O$.



**OCIS codes:** (130.6010) Integrated Optics: Sensors; (300.1020) Spectroscopy: Absorption; (300.6340) Spectroscopy, infrared; (300.6360) Spectroscopy, laser.

## References and links

1. M. Frish, R. Shankar, I. Bulu, I. W. Frank, M. C. Laderer, R. T. Wainner, M. G. Allen, and M. Lončar, "Progress Toward Mid-IR Chip-Scale Integrated-Optic TDLAS Gas Sensors," Proc. SPIE **9101**, 8631–8639 (2014).
2. X. Fan, I. M. White, S. I. Shopova, H. Zhu, J. D. Suter, and Y. Sun, "Sensitive optical biosensors for unlabeled targets: A review," Anal. Chim. Acta **620**, 8–26 (2008).
3. Y. Sun and X. Fan, "Optical ring resonators for biochemical and chemical sensing." Anal. Bioanal. Chem. **399**, 205–211 (2011).
4. M. S. Luchansky and R. C. Bailey, "High-Q optical sensors for chemical and biological analysis," Anal. Chem. **84**, 793–821 (2012).
5. M. Sumetsky, R. S. Windeler, Y. Dulashko, and X. Fan, "Optical liquid ring resonator sensor," Opt. Express **15**, 14376–14381 (2007).
6. A. L. Washburn, M. S. Luchansky, A. L. Bowman, and R. C. Bailey, "Quantitative, label-free detection of five protein biomarkers using multiplexed arrays of silicon photonic microring resonators," Anal. Chem. **82**, 69–72 (2010).
7. F. Vollmer and S. Arnold, "Whispering-gallery-mode biosensing: label-free detection down to single molecules," Nat. Methods **5**, 591–596 (2008).
8. A. Ramachandran, S. Wang, J. Clarke, S. Ja, D. Goad, L. Wald, E. Flood, E. Knobbe, J. Hryniewicz, S. Chu, D. Gill, W. Chen, O. King, and B. Little, "A universal biosensing platform based on optical micro-ring resonators," Biosens. Bioelectron. **23**, 939–944 (2008).
9. O. Scheler, J. T. Kindt, A. J. Qavi, L. Kaplinski, B. Glynn, T. Barry, A. Kurg, and R. C. Bailey, "Label-free, multiplexed detection of bacterial tmRNA using silicon photonic microring resonators," Biosens. Bioelectron. **36**, 56–61 (2012).
10. C. F. Carlborg, K. B. Gylfason, A. Kazmierczak, F. Dortu, M. J. Banuls Polo, A. Maquieira Catala, G. M. Kresbach, H. Sohlström, T. Moh, L. Vivien, J. Popplewell, G. Ronan, C. A. Barrios, G. Stemme, and W. van der Wijngaart, "A packaged optical slot-waveguide ring resonator sensor array for multiplex label-free assays in labs-on-chips," Lab Chip **10**, 281–290 (2010).
11. K. D. Vos, I. Bartolozzi, E. Schacht, P. Bienstman, and R. Baets, "Silicon-on-insulator microring resonator for sensitive and label-free biosensing," Opt. Express **15**, 7610–7615 (2007).
12. A. Ksendzov and Y. Lin, "Integrated optics ring-resonator sensors for protein detection," Opt. Lett. **30**, 3344–3346 (2005).

#229046 - $15.00 USD Received 4 Dec 2014; revised 12 Jan 2015; accepted 24 Jan 2015; published 23 Feb 2015

13. N. A. Yebo, P. Lommens, Z. Hens, and R. Baets, "An integrated optic ethanol vapor sensor based on a silicon-on-insulator microring resonator coated with a porous ZnO film," Opt. Express **18**, 11859–11866 (2010).
14. T. H. Stievater, M. W. Pruessner, D. Park, W. S. Rabinovich, R. A. McGill, D. A. Kozak, R. Furstenberg, S. A. Holmstrom, and J. B. Khurgin, "Trace gas absorption spectroscopy using functionalized microring resonators," Opt. Lett. **39**, 969–972 (2014).
15. A. M. Armani and K. J. Vahala, "Heavy water detection using ultra-high-Q microcavities," Opt. Lett. **31**, 1896–1898 (2006).
16. A. Nitkowski, L. Chen, and M. Lipson, "Cavity-enhanced on-chip absorption spectroscopy using microring resonators," Opt. Express **16**, 11930–11936 (2008).
17. J. T. Robinson, L. Chen, and M. Lipson, "On-chip gas detection in silicon optical microcavities," Opt. Express **16**, 4296–4301 (2008).
18. W. G. Jr., Y. Hidaka, and T. Tanzawa, "Refractivity of combustion gases," Combust. Flame **40**, 213–219 (1981).
19. "The HITRAN Database," http://www.cfa.harvard.edu/hitran/.
20. C. Y. Wang, T. Herr, P. Del'Haye, a. Schliesser, J. Hofer, R. Holzwarth, T. W. Hänsch, N. Picqué, and T. J. Kippenberg, "Mid-infrared optical frequency combs at 2.5$\mu$m based on crystalline microresonators." Nat. Commun. **4**, 1345 (2013).
21. R. Soref, "Mid-infrared photonics in silicon and germanium," Nature Photon. **4**, 495–497 (2010).
22. R. A. Soref, S. J. Emelett, and W. R. Buchwald, "Silicon waveguided components for the long-wave infrared region," J. Opt. A: Pure Appl. Opt. **8**, 840 (2006).
23. Y. Xia, C. Qiu, X. Zhang, W. Gao, J. Shu, and Q. Xu, "Suspended Si ring resonator for mid-IR application," Opt. Lett. **38**, 1122–1124 (2013).
24. Z. Cheng, X. Chen, C. Y. Wong, K. Xu, and H. K. Tsang, "Mid-infrared suspended membrane waveguide and ring resonator on silicon-on-insulator," IEEE Photon. J. **4**, 1510–1519 (2012).
25. R. Shankar, I. Bulu, and M. Lončar, "Integrated high-quality factor silicon-on-sapphire ring resonators for the mid-infrared," Appl. Phys. Lett. **102**, 051108 (2013).
26. A. Spott, Y. Liu, T. Baehr-Jones, R. Ilic, and M. Hochberg, "Silicon waveguides and ring resonators at 5.5$\mu$m," Appl. Phys. Lett. **97**, 213501 (2010).
27. F. Li, S. D. Jackson, C. Grillet, E. Magi, D. Hudson, S. J. Madden, Y. Moghe, C. O'Brien, A. Read, S. G. Duvall, P. Atanackovic, B. J. Eggleton, and D. J. Moss, "Low propagation loss silicon-on-sapphire waveguides for the mid-infrared," Opt. Express **19**, 15212–15220 (2011).
28. A. Yariv, "Universal relations for coupling of optical power between microresonators and dielectric waveguides," Electron. Lett. **36**, 321–322 (2000).
29. T. J. Kippenberg, S. M. Spillane, and K. J. Vahala, "Modal coupling in traveling-wave resonators," Opt. Lett. **27**, 1669–1671 (2002).

## 1. Introduction

As emissions and atmospheric trace-gas monitoring becomes increasingly important due to concerns about climate change, the need for robust, highly sensitive, easily mass-produced spectrometers has increased. Laser-based trace-gas spectrometers are technically promising, but their costs are high, driven primarily by multiple device packaging steps for the spectrometer's constituent components (especially the laser and detector). A potential solution is the development of novel gas sensing elements using microscale low-loss resonant waveguide ring resonators which can be integrated into a compact package suitable for inexpensive mass production [1]. For trace-gas spectrometers based on a ring resonator design to be successfully mass produced, the design must be compatible with: 1) Reliable production of high quality factor ($Q$) resonant structures via a high-volume commercial semiconductor fabrication process; 2) Conventional micro-optic, semiconductor, and electronic assembly techniques to package the laser, detector, and sensing element; and 3) Use in the mid-wavelength (MWIR, 3-8 $\mu$m) and long-wavelength infrared (LWIR, 8-15 $\mu$m) for access to fundamental molecular vibrations.

The conventional analyte measurement methodology employed with ring resonators is to measure the change in visible or near-infrared (NIR) wavelength refractive index (RI) of the waveguide cladding via the ring resonance wavelength shift when the resonator is exposed to an analyte [2–4]. The RI change can be based on a measurement of the bulk RI or the surface RI [5–12]. Measurement of trace-gases with ring resonators has been performed via adsorption of the analyte onto a selective coating (which acts as a concentrator) on the ring resonator (*e.g.*, [13,

#229046 - $15.00 USD Received 4 Dec 2014; revised 12 Jan 2015; accepted 24 Jan 2015; published 23 Feb 2015

14]). However, while functionalizing or coating the waveguide surface is effective at enhancing ring resonator sensitivity to analyte concentration, it is typically an accumulative process which requires a reset mechanism such as flushing [10, 12, 13]. Consequently this approach would not be very effective for a generalized long-term monitoring application in which the analyte concentration is expected to change over time.

An alternative approach to measuring analyte concentration via ring resonance wavelength shift is to measure the change in ring resonance $Q$ due to increased absorption by the analyte, as has been shown by [15, 16]. The primary advantages of this approach are that the optical frequency axis does not need to be calibrated since the shape of the resonance is measured relative to a zero condition and absorption has a stronger effect than dispersion.

Nevertheless, if a gas analyte's dispersion is sufficiently high (due to strong line intensity and/or high concentration), the ring resonance wavelength shift can be measured directly with the gas acting as the cladding, as has been shown via measurement of acetylene in the NIR [17]. In this case, at standard temperature and pressure (STP) and 1527.5 nm optical wavelength, pure acetylene has $\sim 3.24 \times 10^{-4}$ refractive index unit (RIU) difference from air [18]. This results in a ring resonance wavelength shift of $0.19 \pm 0.07$ nm (*i.e.*, $\Delta\lambda/\lambda_0 \approx 1.2 \times 10^{-4}$) for a ring resonator with $Q$ of 5000 (389 $\mu$m effective path length), effective index ($n_{eff}$) of 2.01, and optical mode confinement ($\Gamma$) of 0.64 [17]. In contrast, at its 1528 nm wavelength spectral line, the pure acetylene absorption co-efficient is 0.43 cm$^{-1}$, yielding 1.7% absorption over the 389 $\mu$m effective path length of the device in [17]. Thus the measurable signal produced from absorption (1.7% change from the zero case) is much larger than that produced from dispersion ($1.2 \times 10^{-4}$ from the zero case), enabling higher sensitivity to be achieved by absorption-based vs. dispersion-based sensors (assuming comparable noise).

The primary limitation to sensing trace-gases using bare ring resonator devices in the NIR is that the analyte line strengths are much weaker than those in the MWIR & LWIR because the NIR optical transitions are overtones of the fundamental vibrational modes (which occur in the MWIR & LWIR). For example, at the NIR 1528 nm overtone, the pure acetylene absorption co-efficient is 0.43 cm$^{-1}$; whereas, at the LWIR fundamental $\sim$13.5 $\mu$m wavelength, the absorption co-efficient is $> 20$ cm$^{-1}$ [19]. Many atmospheric gases (*e.g.*, $CO_2$, $N_2O$, $H_2O$, *etc.*) in pure concentrations have absorption co-efficients in the MWIR & LWIR that are $>10$ cm$^{-1}$; however, the challenge in measuring them is they occur in trace-concentrations – parts-per-billion to parts-per-million by volume (ppbv-ppmv) – thereby greatly reducing their path integrated absorbance. With the emergence of MWIR & LWIR quantum and intersubband cascade lasers (QCLs and ICLs), cost-effective integrated-optic trace-gas sensing with ring resonators may be practical.

Another challenge regarding use of ring resonators in the MWIR is material selection. Ultra-high $Q$ ($> 10^8$) resonators in MWIR-transparent glasses like $MgF_2$ and $CaF_2$ can be fabricated [20], though these devices require fiber coupling and are not as easily integrated as Si devices are. Though poorly appreciated for MWIR applications, given its low material losses below 8 $\mu$m wavelength and semiconductor mass production compatibility, Si itself is a promising waveguide candidate for ring resonator structures [21,22]. However, $SiO_2$ has $>2$ dB/cm losses at wavelengths longer than 3.5 $\mu$m, with the result that many silicon-on-insulator (SOI) ring resonator implementations have had to rely on suspended waveguide structures to effectively operate in the MWIR [23, 24]. On the other hand, successful MWIR waveguide and ring resonator implementations have been shown with the silicon-on-sapphire (SOS) platform [25–27]. Because sapphire has low losses throughout much of the MWIR, it functions properly as a cladding material and enables fabrication of waveguides using less complex techniques.

In this paper we demonstrate that a QCL-interrogated SOS ring resonator can sense dilute $N_2O$. The concentration of the $N_2O$ is deduced via the change in ring resonator $Q$ due to losses

#229046 - $15.00 USD Received 4 Dec 2014; revised 12 Jan 2015; accepted 24 Jan 2015; published 23 Feb 2015

via absorption of the evanescent wave of the optical mode traveling in the waveguide.

## 2. Theory

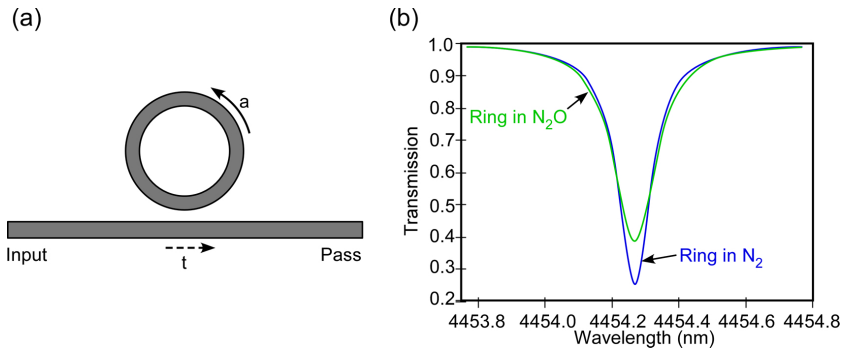


Fig. 1. (a) Schematic of an all-pass ring resonator. $a$ is the field attenuation co-efficient and $t$ is transmission co-efficient. (b) Simulation of ring resonator spectra showing the impact on the ring resonator $Q$ of 5% $N_2O$.

Traditional laser-based spectrometers measure trace-gas concentration through the change in light intensity ($I/I_0$) due to absorption by gas with absorption co-efficient ($\alpha_{gas}$) over a path length, $L$, according to the Beer-Lambert law, $I/I_0 = e^{-\alpha_{gas}L}$. A ring resonator (Fig. 1(a)) can measure the concentration of a gas through its absorption of the optical mode's evanescent field, which reduces the resonator's $Q$ (Fig. 1(b)) through the impact of the absorber on the attenuation co-efficient, $a$, of the resonator. In general, the shape of the transmitted light intensity ($T(\lambda)$) by an all-pass ring resonator as a function of wavelength can be described by [16, 28]:

$$T(\lambda) = \frac{a^2 + |t|^2 - 2a|t|\cos(\lambda)}{1 + a^2 + |t|^2 - 2a|t|\cos(\lambda)} \tag{1}$$

where,

$$\cos(\lambda) \approx 1 - \frac{2\pi^2 L^2 n_g^2}{\lambda_0^4}(\lambda - \lambda_0)^2 \tag{2}$$

$L$ is the length (cm) of the ring ($L = 2\pi r$), $n_g$ is the group waveguide index, $\lambda_0$ is the free-space light wavelength at the ring-resonance, $\lambda$ is the free-space wavelength (cm) of light, $a$ is the attenuation co-efficient, and $t$ is the transmission co-efficient.

When placed in an environment with an absorbing gas, the power attenuated in one round trip of the ring can be described as a combination of waveguide losses and loss due to absorption from the gas:

$$\alpha_{tot} = \alpha_I + \Gamma\alpha_{gas} \tag{3}$$

Where $\alpha_I$ is the intrinsic loss ($cm^{-1}$) of the waveguide, $\alpha_{gas}$ is the absorption coefficient ($cm^{-1}$) of the gas, and $\Gamma$ is a scaling term to account for the optical mode confinement within the waveguide (this can be estimated empirically or through simulation via [17]).

The gas absorption co-efficient, $\alpha_{gas}$, is defined by:

$$\alpha_{gas}(\lambda, T) = S(\lambda, T)G(\lambda - \lambda_0)N \tag{4}$$

#229046 - $15.00 USD Received 4 Dec 2014; revised 12 Jan 2015; accepted 24 Jan 2015; published 23 Feb 2015

Where $S(\lambda, T)$ is the temperature-dependent line strength (cm) of the gas, $G(\lambda - \lambda_0)$ is the absorption line profile (cm), and $N$ is the gas molecule number density (molecules/cm$^3$) which is dependent on temperature and pressure through the ideal gas law.

The attenuation co-efficient for a ring resonator in the presence of an absorbing gas is described using the Beer-Lambert Law:

$$a_{gas}^2 = \frac{I}{I_0} = e^{-\alpha_{tot} L} \tag{5}$$

From Eq. (1) the transmission intensity of the ring resonator in the presence of an absorbing analyte is:

$$T(\lambda) = \frac{a_{gas}^2 + |t|^2 - 2a_{gas}|t|\cos(\lambda)}{1 + a_{gas}^2 + |t|^2 - 2a_{gas}|t|\cos(\lambda)} \tag{6}$$

By convention, $Q$ (defined as the ratio of resonance wavelength to linewidth) is the figure of merit used to quantify the sharpness of a resonator's shape; consequently, it is useful to express Eq. (1) in terms of $Q$ based on [29]:

$$t = \frac{\frac{\omega_0}{2Q_0} - \frac{\omega_0}{2Q_c} - i\Delta\omega}{\frac{\omega_0}{2Q_0} + \frac{\omega_0}{2Q_c} - i\Delta\omega} \tag{7}$$

$$T = tt^* \tag{8}$$

$$\frac{1}{Q_{cav}} = \frac{1}{Q_0} + \frac{1}{Q_c} \tag{9}$$

Here, $\omega_0$ is the system's resonance frequency, $\Delta\omega$ is the deviation from the resonance frequency, $Q_0$ is the intrinsic $Q$ of the ring resonator, $Q_c$ is the coupling quality factor between the ring and the waveguide, and $Q_{cav}$ is the total quality factor (coupling + intrinsic) of the ring resonator in zero gas conditions. The overall quality factor ($Q_{tot}$) of the ring resonator in the presence of an analyte can be described by:

$$\frac{1}{Q_{tot}} = \frac{1}{Q_{cav}} + \frac{1}{Q_{abs}}, \textit{where } \frac{1}{Q_{abs}} = \frac{\Gamma\alpha_{gas}\lambda_0}{2\pi n_{eff}} \tag{10}$$

To meet the challenge of ppmv-level sensitivity, it is highly important that ring resonator sensors maximize the interaction volume (path length and cross-sectional area) of the evanescent wave with the trace-gas analyte. The waveguide $\Gamma$ and the ring resonator $Q$ are the primary design parameters available for maximizing the interaction of the evanescent wave with the analyte. Unfortunately, these two parameters can be at odds: A ring resonator with low confinement will have greater evanescent wave interaction with the analyte; however, ring resonator surface defects will more negatively impact the quality factor. The free space equivalent path length, $L_{eff}$, is a useful metric for assessing the detection limit of a ring resonator (or determining the properties of a ring resonator to meet a goal detection limit):

$$L_{eff} = \Gamma\frac{Q\lambda_0}{2\pi n_{eff}} \tag{11}$$

#229046 - $15.00 USD Received 4 Dec 2014; revised 12 Jan 2015; accepted 24 Jan 2015; published 23 Feb 2015

## 3. Experimental setup

A modified version of the ring resonator design in [25] was used to measure $N_2O$, as its parameters were already optimized for operation at 4.4-4.5 $\mu$m wavelength. The original design ($n_{eff} = 2.3$ and $\Gamma = 0.1$) had a radius of 60 $\mu$m, which resulted in a free spectral range (FSR) of $\sim$6.2 cm$^{-1}$ (12.4 nm). To increase the probability of a ring resonance intersecting with an $N_2O$ absorption line (having linewidth $\sim$0.2 cm$^{-1}$), modified ring resonator waveguides were fabricated having 120 $\mu$m radius and FSR of $\sim$3.1 cm$^{-1}$ (6.2 nm).

Fig. 2(a) is a schematic of the experimental setup. To evaluate the waveguide microring resonator structures, they were interrogated within a controlled gas environment (at STP flushed with $\sim$50 sccm flow rate) by a laser beam from an external cavity QCL-based (EC-QCL) MWIR source (Daylight Solutions) emitting (with linewidth $< 0.002$ cm$^{-1}$) at $\sim$4.27-4.63 $\mu$m wavelength, enabling probing of the fundamental R-branch of $N_2O$. The EC-QCL was tuned at a rate of $\sim$1.75 cm$^{-1}$/s.

A focusing lens (NA = 0.22) coupled the free-space light from the EC-QCL into the input grating at normal incidence. The estimated coupling efficiency is $\sim$4% with $\sim$1 mW power circulating in the device. The output of the waveguide (far-field shown in Fig. 2(b)) was collected by a 0.5 NA collimation lens and directed to an MCT detector (Vigo). The detector signal was collected and digitized by a NI USB-6251 DAQ (1.7 MHz acquisition bandwidth). A custom LabVIEW program was used to control the EC-QCL, collect, and save the data.

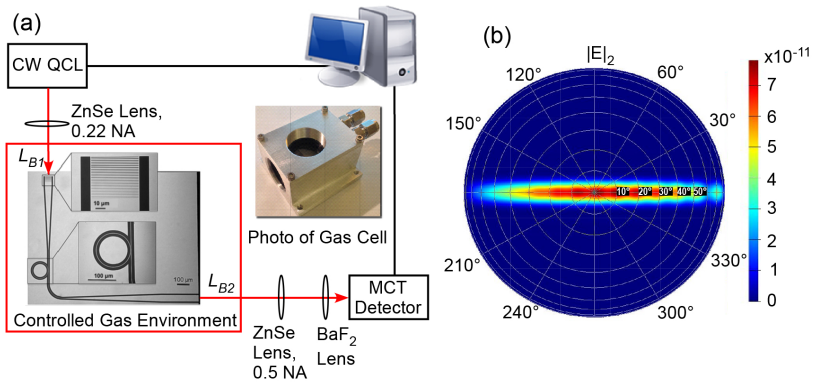


Fig. 2. (a) Schematic of experimental setup showing the beam path, optical elements, and the free-space background paths within the controlled gas environment. (Inset: Picture of the custom gas cell for evaluation of ring resonator chips.) (b) Far-field emission (intensity in A.U.) of the SOS waveguide device.

A custom sealed aluminum gas sampling cell (inset of Fig. 2(a)) with optical interrogation ports (1 mm thick, 2.54 cm diameter $CaF_2$ windows) was fabricated to minimize the free-space optical path within the controlled gas environment. The cell has both vertical and lateral view ports, allowing for simultaneous edge-on and normal interrogation of the SOS substrate within the calibrated gas environment. Effort was made to minimize distance between interrogation windows both normal and edge-on to the substrate to allow the closest possible placement of both focusing and collection optics.

Despite efforts to minimize dead space within the cell, the MWIR beam traversed approximately 2 cm (depicted as $L_{B1}$ and $L_{B2}$ in the schematic of Fig. 2(a)) $N_2O$ in the space between interrogation windows and substrate. Consequently, this results in an additional $N_2O$ absorption signal, as shown in Fig. 3(a). A challenge which arises from the use of a high index waveguide is the presence of background fringes arising from the waveguide itself, the effects of which are

#229046 - $15.00 USD Received 4 Dec 2014; revised 12 Jan 2015; accepted 24 Jan 2015; published 23 Feb 2015

illustrated in Fig. 3(a). For these devices, the waveguide dimensions lead to fringes with FSR corresponding to 1 cm length scale. An additional, higher frequency fringe can also be observed in Fig. 3(b). The length scale of this fringe corresponds to approximately 2 m. It is believed that this fringe arises from the experimental apparatus itself (likely from the EC-QCL). Such fringes limit the sensitivity of the present setup. Future measures to suppress such fringes include using a DFB QCL, applying an anti-reflection (AR) coating to the waveguide output facet, and designing the output waveguide direction to be non-orthogonal with the crystallographic plane used for cleaving.

Additionally, the EC-QCL exhibited an inconsistent, non-linear scan rate, which caused the reported optical frequency to exhibit up to 0.05 $cm^{-1}$ differences among scans spanning across a known spectral absorption line (Fig. 3(b)), complicating the process of comparing lineshapes among successive scans. To overcome this, the HITRAN database was used for frequency-axis calibration; however, this method was limited to the case in which the $N_2O$ absorption features were distinguishable from the fringes (*e.g.*, 5000 ppmv).

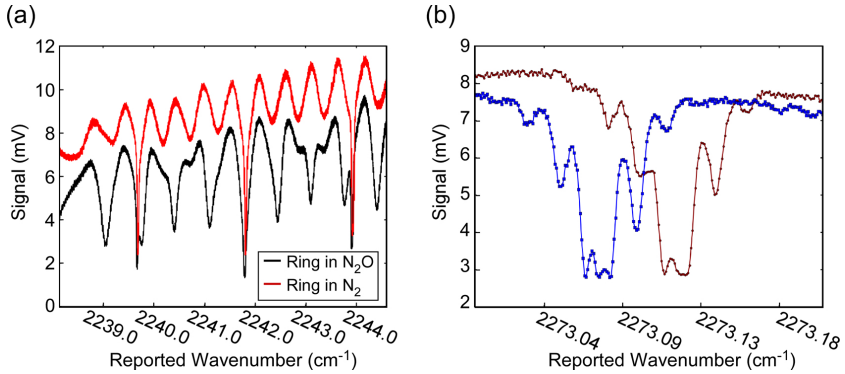


Fig. 3. (a) Transmission spectra of ring resonators in an $N_2O$ and zero gas ($N_2$) environment showing both impact of fringes from the waveguide and the background $N_2O$ absorption. (b) The $\sim$0.05 $cm^{-1}$ scan-to-scan error of the external cavity QCL is also demonstrated.

## 4. Results and discussion

Because the background $N_2O$ absorption signal was approximately 60%, waveguide devices on a given chip were made both with and without ring resonators so that the effect of $N_2O$ attenuation on the ring resonator signal could be isolated. Spectra from waveguide devices both with and without ring resonators can be seen in Fig. 4(a). Isolation of the ring resonator signal was done by taking a background $N_2O$ absorption correction spectrum. The corrected $N_2O$ background spectrum was created by normalizing the $N_2O$ absorption spectrum from a device without a ring with a zero gas spectrum from the same device. This normalization reduced many of the large transmission effects due to fringes, coupling loss, *etc.* The resulting spectrum was then frequency-axis calibrated and fit (Fig. 4(b)) to HITRAN via non-linear least squares optimization for further suppression of the effects of noise and fringes.

The resulting fit enabled suppression of the background $N_2O$ absorption in the ring resonator signal without introduction of additional noise and fringes. This was done by dividing the total transmission spectrum (with ring resonance) by the full spectral fit (Fig. 4(b)) of the $N_2O$ background spectrum (without a ring resonance). Once the ring resonator signal was isolated, its response to $N_2O$ concentration was compared to theory (Fig. 5).

This method was found to be effective in isolating the ring resonator signal for the calibrated

#229046 - $15.00 USD Received 4 Dec 2014; revised 12 Jan 2015; accepted 24 Jan 2015; published 23 Feb 2015

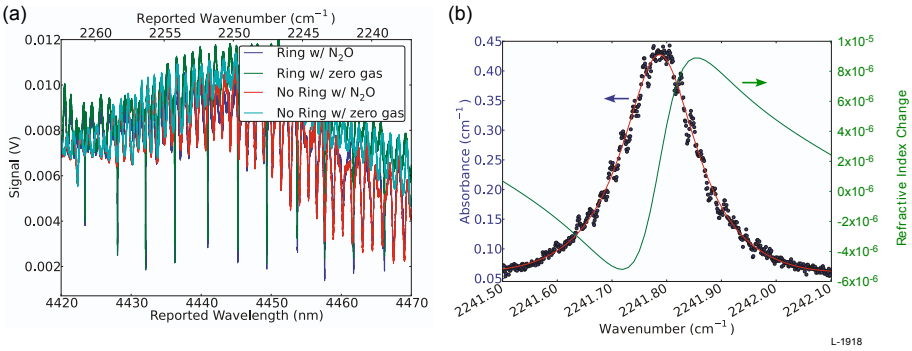


Fig. 4. (a) Spectra of waveguides with and without ring resonators in the presence of both $N_2O$ and zero gas. (b) $N_2O$ background absorbance experimental data with fit and calculated dispersion.

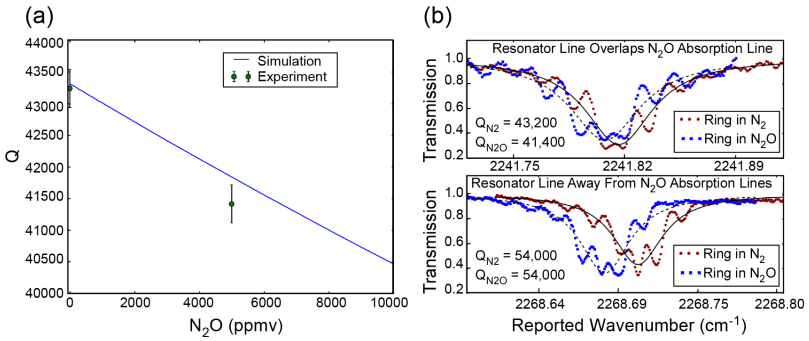


Fig. 5. (a) Comparison to theory of measured ring resonator $Q$ in zero gas and in 5000 ppmv $N_2O$. (b) Background normalized spectral data with fits used for the calculation of ring resonance $Q$ in the presence of $N_2O$. Fits of ring resonance spectra away from an $N_2O$ absorption line show no change vs. the zero gas case.

EC-QCL scans having optical frequency error much smaller than the ring resonance linewidth ($\sim$0.03 cm$^{-1}$). Additionally, the calculated dispersion at the $N_2O$ absorption line peak (Fig. 4(b)) is $\sim 2\times10^{-6}$. According to $\Delta\lambda = \lambda_0(\Gamma/n_{eff})\Delta n_{gas}$ [17], this causes the overlapping ring resonance to shift by $\sim 2\times10^{-4}$ cm$^{-1}$ (well below the frequency resolution in this experiment).

The measurement of the $N_2O$ R23 line at 2241.79 cm$^{-1}$ ($\nu_3$ vibrational band) by the ring resonator device was verified against theory (Fig. 5(a)) by using non-linear least squares optimization to fit the change in $Q$ from the zero gas case to when the ring resonator was placed in a calibrated 5000 ppmv $N_2O$ atmosphere ($\alpha_{gas} \approx 0.45$ cm$^{-1}$). For this device, theory predicts that a 5,000 ppmv $N_2O$ concentration should decrease $Q$ by 3.4% from $\sim$43,300 to $\sim$41,800, while the experimental results show a 4.4% decrease in $Q$ from $\sim$43,200 to $\sim$41,400 (Fig. 5). Analysis of another resonator line (Fig. 5(b)) at a frequency far away from the effects of $N_2O$ shows essentially no change in $Q$ between $N_2O$ and $N_2$ environments. The $L_{eff}$ of the ring at 2241.79 cm$^{-1}$ is $\sim$1 mm, which corresponds to $\sim$5% absorption by 5000 ppmv $N_2O$.

These findings illustrate good agreement between theory and measurement, though elimination of free-space background path and suppression of fringes would lead to improved sensitivity. The waveguide-induced fringes present in the system are approximately 10% of the signal amplitude. While fitting to the shape of the ring resonance overcomes much of the uncertainty

#229046 - $15.00 USD Received 4 Dec 2014; revised 12 Jan 2015; accepted 24 Jan 2015; published 23 Feb 2015

induced by the fringes, performing successive fits to 3-4 sequential scans show $Q$ uncertainties of approximately $\pm 300$, which limits the sensor's precision to approximately $\pm 1000$ ppmv ($\alpha_{gas} \approx 0.09$ cm$^{-1}$).

## 5. Conclusion

Micro-ring resonators show promise in their ability to significantly shrink the size of existing trace-gas detection instruments. We showed the possibility of MWIR gas measurements using a QCL and SOS ring resonator. Currently some of the highest ring resonator $Q$'s demonstrated in the MWIR using SOS waveguides have been on the order of 100,000 [25]. This work demonstrated both in theory and experiment, that $Q \approx 40{,}000$ (determined with precision of $1 \times 10^{-2}$) is sufficient to detect (with $SNR \approx 5$) analytes with absorption coefficients $< 0.5$ cm$^{-1}$, such as 5000 ppmv of $N_2O$.

Future research on this sensing technique should strive to determine $Q$ with $1 \times 10^{-4}$ precision. Potential methods include reducing internal fringing due to Fresnel reflections from waveguide facets via AR coating, designing the waveguide output direction to be non-orthogonal to the crystallographic plane used for cleaving, and integrating the optical components to minimize background absorption. Finally, to achieve sub-ppmv detection limits (assuming $1 \times 10^{-4}$ precision), most trace-gases will require MWIR resonators with $L_{eff} > 1$ cm, which implies $Q >$325,000 for $\Gamma = 0.1$ or $Q >$65,000 for $\Gamma = 0.5$.


## Acknowledgments

This material is based upon work supported by the USA Contracting CMD-APG under Contract Number W911SR-12-C-0041, sponsored by the Edgewood Chem Bio Center.